JOURNAL OF GEOPHYSICAL RESEARCH, VOL. 103, NO. D24, PAGES 32,001–32,011, DECEMBER 27, 1998

# Vegetation detection through smoke-filled AVIRIS images: An assessment using MODIS band passes

T. Miura, A. R. Huete, W. J. D. van Leeuwen, and K. Didan

Department of Soil, Water and Environmental Science, University of Arizona, Tucson

**Abstract.** Radiometrically calibrated, Airborne Visible/Infrared Imaging Spectrometer (AVIRIS) images acquired during the Smoke, Clouds and Radiation in Brazil (SCAR-B) experiment were processed to simulate vegetation index (VI) imagery with the Moderate Resolution Imaging Spectroradiometer (MODIS) band passes. Data sets were extracted from tropical forested areas, burned fields, and shrub/grassland areas over both clear and variable smoke conditions with average aerosol optical thickness (AOT) values at 0.67 μm of 0.14, 1.1, and 1.9, respectively. The atmospheric resistant VIs and various middle-infrared (MIR) derived VIs were then analyzed with respect to their ability to minimize atmospheric "smoke" contamination. The atmospheric resistant VIs utilized the blue band for correction of the red band, while the MIR-derived VIs used the MIR region (1.3 - 2.5 μm) as a substitute for the red band since it is relatively transparent to smoke, yet remains sensitive to green vegetation. The performance of these indices were assessed and compared with the normalized difference vegetation index (NDVI) and the soil-adjusted vegetation index (SAVI). Over the tropical forests the NDVI and SAVI had high relative errors over all smoke-filled atmospheric conditions (50-80% error), while the atmospheric resistant VIs resulted in a 50-80% relative error only over thick levels of smoke. Over optically thin levels (AOT at 0.67 μm < 1.1) they performed much better with a 20-40% relative error. The MIR-derived VIs, on the other hand, outperformed all other VIs over forested areas (≤ 5% error). However, over burned fields with minimal amounts of green biomass the MIR-derived VIs had the highest levels of error due to smoke (> 40%), while all other indices had errors below 20%. In the shrub/grassland site, the atmospheric resistant indices behaved similarly with the MIR-derived indices, with both less sensitive to smoke than the NDVI and SAVI. We conclude that the MIR indices, particularly with MODIS band 7 (2.13 μm), are useful in vegetation monitoring over forested areas during the burning season. However, they did not perform well in areas outside of forests such as burned areas and shrub/grassland.

## 1. Introduction

Vegetation monitoring in the Amazon Basin is of particular interest to the Earth science community. Widespread burning practices have been converting the tropical forests into agricultural fields and cattle pastures. During the last decade the rate of conversion has increased and expanded into the cerrado region as a result of a growing population [*Kaufman et al.*, 1990; *Holben et al.*, 1996]. Nearly 80% of the particulates and trace gases emitted from global biomass burning occur in the Amazon Basin and in Africa [*Crutzen and Andreae*, 1990; *Hao et al.*, 1990]. For these reasons it has become increasingly important to monitor the temporal and spatial changes of such land-use practices in order to understand and predict ecosystem response and quantity of emission products.

Regional to global monitoring of terrestrial vegetation currently involves the use of spectral vegetation indices (VIs) as measured from satellite remote sensors. The most widely used in global vegetation studies has been the normalized difference vegetation index (NDVI), which is the difference of the near-infrared (NIR) and red bands divided by their sum [e.g., *Tucker*, 1979]. The NDVI has been successfully utilized in phenological studies of the vegetation growing season, land cover classification, and global climate modeling [*Justice et al.*, 1985; *Townshend et al.*, 1991; *Sellers, et al.*, 1994]. Several improved VI equations have also been developed in order to improve upon the NDVI through removal of canopy background noise, atmospheric contamination, and saturation problems inherent in the NDVI. The soil- and atmospheric-correcting NDVI variants include the soil-adjusted vegetation index (SAVI) [*Huete*, 1988], the atmospherically resistant vegetation index (ARVI) [*Kaufman and Tanré*, 1992], and the soil-adjusted/atmospherically resistant vegetation index (SARVI) [*Huete et al.*, 1997]. All of the NDVI variants have been shown to outperform the NDVI in decreasing canopy background noise and/or atmospheric noise relative to the NDVI signal in numerous studies involving simulated, airborne, and satellite data sets [*Huete et al.*, 1994, 1997].

Vegetation detection in the Amazon Basin using remotely sensed data, however, continues to be problematic due to smoke from biomass burning as well as clouds and saturation problems associated with the NDVI equation [*Goward et al.*, 1991; *Huete et al.*, 1997]. Biomass burning occurs during the dry season, which can last 5 months, and is the most intense



Paper number 98JD00051.
0148-0227/98/98JD-00051$09.00

in August and September [*Andreae*, 1991; *Holben et al.*, 1996]. During these periods, the basin is covered by smoke from biomass burning, and the optical thickness and properties of aerosols vary greatly both temporally and spatially [*Holben et al.*, 1996]. The complexity of vegetation detection through smoke also arises from the high sensitivity of the chlorophyll absorption region to smoke [*Kaufman and Remer*, 1994].

Various suggestions have been made to correct for aerosols on a pixel-by-pixel basis. One approach is to utilize the blue band for correction of the red band, known as the "atmospheric resistance" concept [*Kaufman and Tanré*, 1992]. The atmospheric resistant variants of the NDVI include the ARVI and SARVI. A second approach is to use the middle-infrared (MIR) wavelength region (1.3-2.5 μm) in place of the red band since the longer wavelengths are much less sensitive to smoke, yet remain sensitive to differences in vegetation [*Kaufman and Remer*, 1994]. *Kaufman and Remer* [1994] showed the usefulness of the MIR channel (3.75 μm) in the NOAA Advanced Very High Resolution Radiometer (AVHRR) sensor series for detection of dark, dense vegetation.

In this study, we evaluated the performance of the "atmospheric resistant" VIs in smoke-filled atmosphere conditions. We also analyzed the performance of the "MIR-derived" VIs in order to assess their utility and capabilities in vegetation detection and monitoring in smoke-filled atmospheres. In addition, the NDVI and its soil-correcting variant, SAVI, were evaluated for comparison. These indices were analyzed over three land cover conditions through variable smoke contamination, including open tropical forest, burned fields, and shrub/grassland.

## 2. Methods

The study areas were located in open tropical forest (Alta Floresta and Ji-Parana) and cerrado areas (Cuiaba) in the Amazon Basin where Airborne Visible/Infrared Imaging Spectrometer (AVIRIS) images were acquired during the Smoke, Clouds and Radiation in Brazil (SCAR-B) experiment in August 1995 (Figure 1). The areas were covered by optically thick smoke resulting from active biomass burning of the tropical forest. The reported daily average values of aerosol optical thickness (AOT) at 0.67 μm were 1.1 and 1.9 in Alta Floresta and Ji-Parana, respectively. Relatively smoke-free AVIRIS images (AOT at 0.67 μm of 0.14) were acquired near Cuiaba to be used as a reference. Table 1 summarizes the spectral AOT values, interpolated from Sun photometer data taken every 15 min.

The AVIRIS images were first convolved to the first seven MODIS band passes (Table 2) and normalized to "top-of-atmosphere", apparent reflectances by their exoatmospheric solar irradiances. Corrections for Rayleigh scattering and ozone absorption were made with the 6S radiative transfer code [*Vermote et al.*, 1995] using the equation [*Tanré et al.*, 1992]

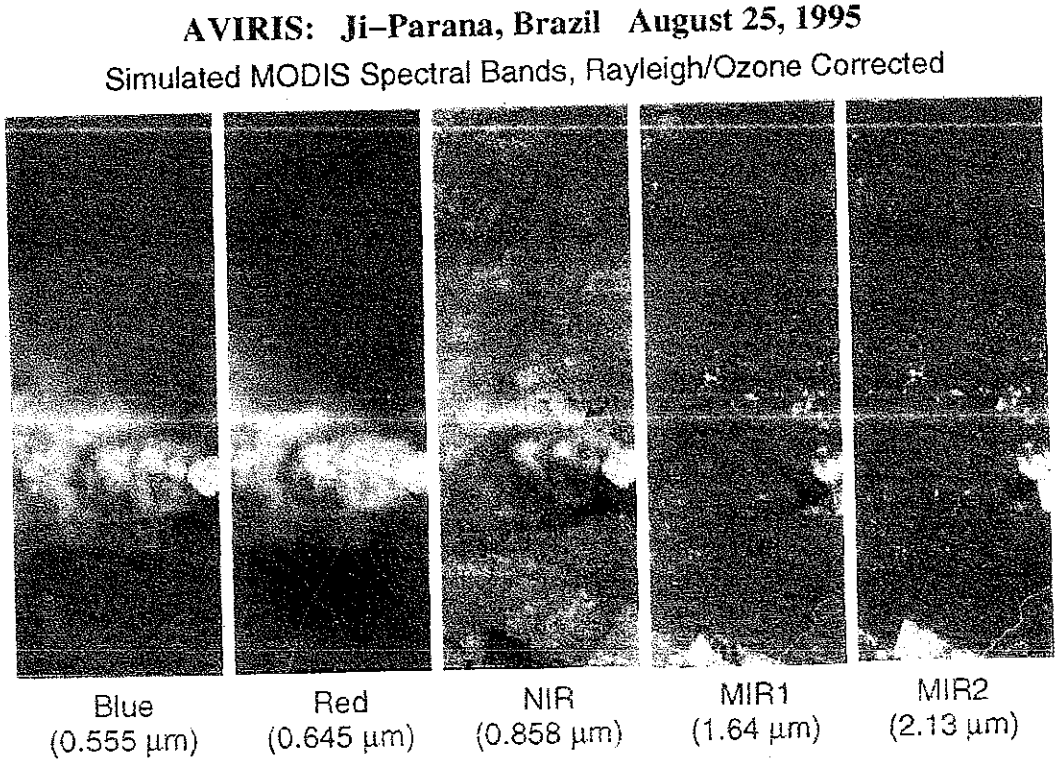


**Figure 1.** Simulated Moderate Resolution Imaging Spectroradiometer (MODIS) band pass images from Airborne Visible/Infrared Imaging Spectrometer (AVIRIS) showing optical properties of smoke aerosols. The AVIRIS image was acquired over Ji-Parana, Brazil, during the SCAR-B experiment on August 25, 1995.

**Table 1.** Spectral Aerosol Optical Thickness (AOT) on the Day of Image Acquisitions

| | Alta Floresta 09°55'S, 56°00'W, Alt. 175 m 20 August 1995 | | | Ji-Parana 10°51'S, 61°47'W, Alt. 100 m 25 August 1995 | | | Cuiaba 15°30'W, 56°00'W, Alt. 250 m 23 August 1995 | | |
|---|---|---|---|---|---|---|---|---|---|
| Wavelength, μm | Daily Average | s.d.[1] | Inst.[2] | Daily Average | s.d. | Inst.[3] | Daily Average | s.d. | Inst. |
| 0.437 | 2.25 | ±1.05 | 3.78 | 4.00 | ±0.21 | - | 0.29 | ±0.07 | 0.18 |
| 0.669 | 1.10 | ±0.56 | 1.90 | 1.91 | ±0.11 | - | 0.14 | ±0.06 | 0.08 |
| 0.871 | 0.58 | ±0.29 | 1.02 | 1.04 | ±0.05 | - | 0.12 | ±0.05 | 0.09 |
| 1.021 | 0.41 | ±0.19 | 0.68 | 0.66 | ±0.03 | - | 0.09 | ±0.05 | 0.06 |

[1] Standard deviation of the daily averaged spectral AOT.
[2] Instantaneous (Inst.) spectral AOT at the time of the image acquisitions.
[3] Instantaneous spectral AOT for Ji-Parana was not available for a lack of measurements at the time of the image acquisitions.

$$\rho^* = \frac{\frac{\rho^{spp}}{t_g O_3} - \rho^{a,r}}{T_r} \quad (1)$$

where $\rho^*$ is the Rayleigh/ozone-corrected reflectance, $\rho^{spp}$ is the apparent reflectance, $\rho^{a,r}$ is the Rayleigh atmospheric reflectance, $t_g O_3$ is the two-way ozone transmittance (absorption), and $T_r$ is the two-way total Rayleigh transmittance of the atmosphere. The highly spatial-temporal variable nature of smoke restricts the spatial extension of aerosol measurements from a single Sun photometer, rendering aerosol correction impractical.

The atmospheric resistant VIs, the MIR-derived VIs, and the NDVI and SAVI were then calculated from the Rayleigh/ozone-corrected reflectances. The NDVI and SAVI were computed as

$$NDVI = \frac{\rho^*_{NIR} - \rho^*_{red}}{\rho^*_{NIR} + \rho^*_{red}}, \quad (2)$$

$$SAVI = (1+L)\left(\rho^*_{NIR} - \rho^*_{red}\right) \Big/ \left(\rho^*_{NIR} + \rho^*_{red} + L\right), \quad (3)$$

where $\rho^*_{NIR}$ and $\rho^*_{red}$ are the Rayleigh/ozone-corrected reflectances in the NIR and red bands, respectively. $L$ is a canopy background adjustment factor that accounts for differential red and NIR extinction through the canopy [*Huete*, 1988]. In this study, $L = 0.5$ was used.

The atmospheric resistant VIs, ARVI and SARVI, were computed as

$$ARVI = \frac{\rho^*_{NIR} - \rho^*_{rb}}{\rho^*_{NIR} + \rho^*_{rb}}, \quad (4a)$$

**Table 2.** MODIS Band Passes and Center Wavelengths

| | Band | Band Pass, μm | Center Wavelength, μm |
|---|---|---|---|
| Blue | 3 | 0.459 - 0.479 | 0.469 |
| Green | 4 | 0.545 - 0.565 | 0.555 |
| Red | 1 | 0.620 - 0.670 | 0.645 |
| NIR | 2 | 0.841 - 0.876 | 0.859 |
| NIR2 | 5 | 1.230 - 1.250 | 1.24 |
| MIR1 | 6 | 1.628 - 1.652 | 1.64 |
| MIR2 | 7 | 2.105 - 2.155 | 2.13 |

where

$$\rho^*_{rb} = \rho^*_{red} - \gamma\left(\rho^*_{blue} - \rho^*_{red}\right), \quad (4b)$$

$$SARVI = G\left(\rho^*_{NIR} - \rho^*_{red}\right) \Big/ \left(L + \rho^*_{NIR} + C_1\rho^*_{red} - C_2\rho^*_{blue}\right), \quad (5)$$

where $\rho^*_{blue}$ is the Rayleigh/ozone-corrected reflectance in the blue band. The $\gamma$ function of ARVI (equation (4b)) corrects aerosol effects in the red band using the difference between the blue and the red bands [*Kaufman and Tanré*, 1992]. As suggested by *Kaufman and Tanré* [1992], we used $\gamma = 1$ in this study. The coefficient $L$ in the SARVI equation (equation (5)) is a canopy background adjustment factor, $C_1$ and $C_2$ adjust the red reflectances for aerosols, and $G$ is a gain factor. We used $L = 1$, $C_1 = 6$, $C_2 = 7.5$, and $G = 2.5$ as used by *Huete et al.* [1997].

The MIR-derived VIs, $NDVI_{MIR}$ and $SAVI_{MIR}$, were computed with both MODIS bands 6 and 7. The MIR1-derived VIs were computed as

$$NDVI_{MIR1} = \frac{\rho^*_{NIR} - \rho^*_{MIR1}}{\rho^*_{NIR} + \rho^*_{MIR1}}, \quad (6)$$

$$SAVI_{MIR1} = (1+L)\left(\rho^*_{NIR} - \rho^*_{MIR1}\right) \Big/ \left(\rho^*_{NIR} + \rho^*_{MIR1} + L\right), \quad (7)$$

where $\rho^*_{MIR1}$ is the MIR1, Rayleigh/ozone-corrected reflectance (MODIS band 6). For the $NDVI_{MIR2}$ and $SAVI_{MIR2}$, $\rho^*_{MIR1}$ in equations (6) and (7) were replaced by the MIR2 reflectance (MODIS band 7) $\rho^*_{MIR2}$.

Three land cover types were identified both under variable smoke contamination and near the Sun photometer sites. These included open tropical forest areas, burned fields, and shrub/grassland areas. The open tropical forest consisted of an overstory of trees with a densely vegetated understory. The shrub/grassland sites were extracted from recently abandoned forest clearings. For each of these land cover types, data were extracted in 12-by-12 (20 m pixel) windows over uniform areas within the images. One set of data was extracted close to the Sun photometer sites, and additional data were extracted over variable smoke contamination for the same land cover type. Pixels inside the smoke plume were also extracted and used for a reference case of maximum AOT.

For each land cover type, the percent relative error $\varepsilon_r$ was used as a means of quantitatively comparing differences

among VI responses under variable levels of smoke contamination [*Huete et al.*, 1994]:

$$\varepsilon_r(\%) = 100\left|VI_p - VI\right| / \left|VI_{max} - VI_{min}\right| , \quad (8)$$

where $VI$ is the "true" VI value (clear conditions), $VI_p$ is the perturbed VI response (smoke contaminated), and $VI_{max}$ and $VI_{min}$ are the maximum and minimum VI values for the VI of interest. The denominator in equation (8) is to standardize the widely differing dynamic ranges of the VIs. The mean of the VI values from the Cuiaba images (clear conditions) was used as the "true" VI value. The mean of the VI values for the forested areas from the Cuiaba images were used for $VI_{max}$ while the burned fields from the Ji-Parana images (smoke contaminated) were used for $VI_{min}$. The percent relative errors were calculated both for the data set extracted near the Sun photometer sites and for the data set over the smoke plume.

## 3. Results

### 3.1 Forested Areas

We first analyzed VI responses over the open tropical forest areas. The Rayleigh/ozone-corrected reflectance spectra under the different smoke aerosol optical thickness conditions are summarized in Figure 2. Reflectances in all three visible bands increased with increases in aerosol optical thickness with red reflectances increasing up to 0.20 units. In contrast, there were only slight increases in the NIR and MIR bands with increasing aerosol optical thickness.

In Figure 3, the NDVI, SAVI, and atmospheric resistant VIs are plotted against the red reflectances in order to assess VI behavior with increasing aerosol optical thickness (red reflectances). In general, all the VI values decreased with smoke contamination with the NDVI decreasing by 0.7 units (0.8 - 0.1) (Figure 3a). This was due mainly to the large increase in red reflectances with smoke with only slight changes in the NIR reflectances (Figure 2), which greatly lowered NDVI values.

The atmospheric resistant VIs were less affected by smoke contamination at the lower optical thickness (AOT at 0.67 μm < 1.1) but remained sensitive to smoke at higher optical thickness (Figures 3c, 3d). Differences between smoke-free pixels and smoke-contaminated pixels (AOT at 0.67 μm ~ 1.1) were lower with the ARVI compared with NDVI (Figure 3c). The SARVI successfully removed aerosol effects for thin smoke with VI values close to the "true" VI values (~ 0.45) (Figure 3d). Both ARVI and SARVI were unable to remove aerosol effects throughout the range of smoke thickness values examined here, particularly at the highest optical thickness conditions.

The MIR-derived VIs, on the other hand, were transparent to smoke (Figure 4). All of the MIR-derived VIs maintained nearly constant values throughout the range of smoke contamination examined here. The MIR1-derived VIs showed more secondary variations (scatter) than the MIR2-derived VIs, and the MIR-derived NDVI values showed more variation than the MIR-derived SAVI values. The reason for the larger amount of scatter in the MIR indices is not clear but may be associated with moisture or structural differences within the forest canopies.

### 3.2 Burned Fields

In this section, we repeat the above analyses over burned fields in order to assess VI behavior over smoke in areas with little or no vegetation. The Rayleigh/ozone-corrected reflectance spectra are shown in Figure 5. For this land cover condition, large increases in reflectances occurred both in the visible and in the NIR bands. The red and NIR reflectances increased by 0.19 units and 0.17 units, respectively, from the smoke-free atmosphere (AOT at 0.67 μm of 0.14) to the dense smoke plume, indicating proportional increases in reflectances for these two bands. There were no large changes in both MIR1 and MIR2 reflectances with maximum differences of 0.02 and 0.03 units, respectively.

Lower influences of smoke were observed with the NDVI, SAVI, and their atmospheric resistant variants over this land

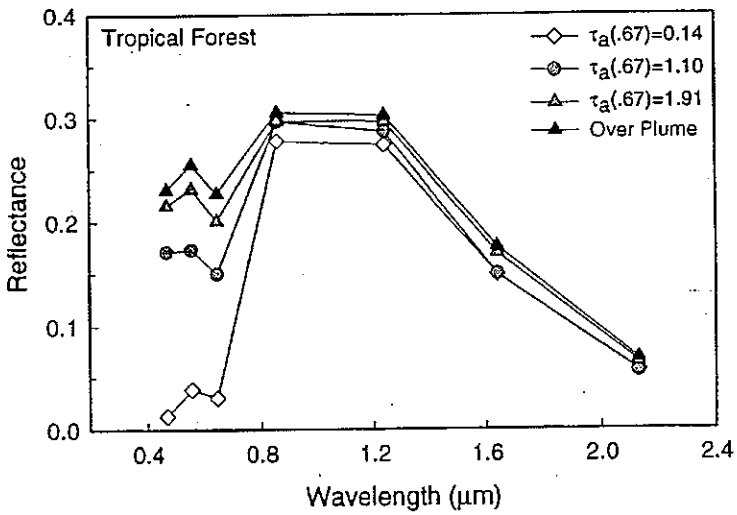


**Figure 2.** Rayleigh/ozone-corrected reflectance spectra of forested areas under four different smoke contaminations. The spectra were extracted near the Sun photometer sites except for the one over the plume. $\tau_a(.67)$ indicates the aerosol optical thickness (AOT) at 0.67 μm.

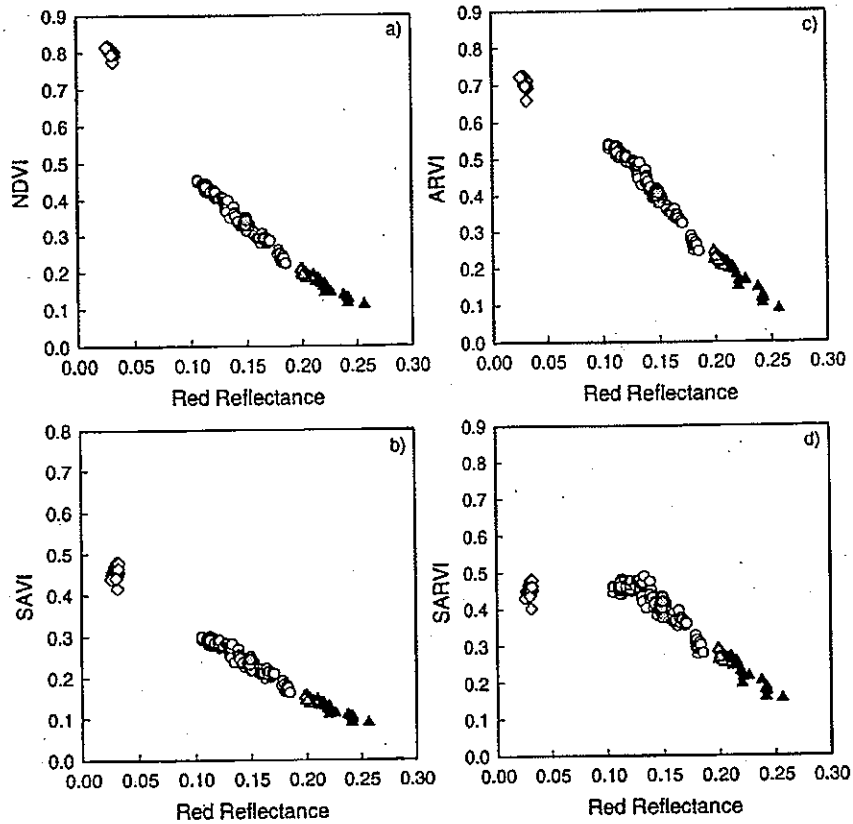


**Figure 3.** Normalized difference vegetation index (NDVI), soil-adjusted vegetation index (SAVI), and atmospheric resistant vegetation indices (VIs) plotted against red reflectances for forested areas. The legend is the same as in Figure 2. The open circles are for pixels extracted under variable smoke contamination.

cover condition (Figure 6). The general tendency was for VI values to decrease with increasing levels of smoke. This was particularly the case of the NDVI and SAVI where maximum values occurred over the smoke-free case (Figures 6a, 6b). The atmospheric resistant VIs behaved differently in that their smoke-free values were not too different from the smoke-contaminated values (Figures 6c, 6d). The SARVI resulted in having nearly constant values (~ 0.07) throughout the range of aerosol optical thickness. The atmospheric resistant VIs appeared to increase slightly and then decrease with increasing aerosol optical thickness (Figures 6c, 6d).

The MIR-derived VIs over burned fields performed worse than the NDVI, SAVI, and atmospheric resistant VIs (Figure 7). All of them displayed a general and consistent increase with increasing smoke contamination. As seen in Figure 5, the NIR reflectances increased with smoke contamination, while the MIR reflectances remained nearly the same, creating a high contrast between these two bands, which resulted in higher VI values. One can also see larger variations in the MIR-derived VIs within a given level of smoke (Figure 7), which may be attributed to moisture, structural, and roughness variations of dead biomass (standing and on the ground).

### 3.3 Shrub/Grassland

The spectral signatures of a shrub/grassland site, representing a vegetation cover intermediate between the two extremes discussed above, were also analyzed (Figure 8). Although the visible and NIR bands increased with smoke contamination, the increase in the NIR reflectance (0.06 units) was much less than in the red reflectance (0.13 units) from the smoke-free to the dense smoke plume. The two MIR bands did not show any large changes in their reflectances, regardless of the aerosol optical thickness.

In Figure 9, the general relationships of the NDVI, ARVI, $NDVI_{MIR1}$, and $NDVI_{MIR2}$ are plotted against red reflectances. The NDVI decreased with increasing smoke contamination (0.3 units from the smoke-free condition to the smoke plume) (Figure 9a), while the ARVI showed fewer variations than the NDVI (Figure 9b). However, the ARVI slightly increased before decreasing in values with increasing smoke contamination (Figure 9b). The $NDVI_{MIR1}$ and $NDVI_{MIR2}$ increased with smoke contamination (0.1 and 0.15 units, respectively) (Figures 9c, 9d). There was no significant difference in the behavior between the $NDVI_{MIR1}$ and the $NDVI_{MIR2}$ with increasing aerosol optical thickness. The SAVI, SARVI, and MIR-derived SAVI had identical patterns as the NDVI, ARVI, and MIR-derived NDVI, respectively, for this land cover type with correlation coefficients between the pairs exceeding 0.98.

### 3.4 Percent Relative Errors

A summary of smoke-induced relative errors for each of the three land cover types is shown in Figure 10. For the forested areas the MIR-derived VIs had considerably smaller errors (≤

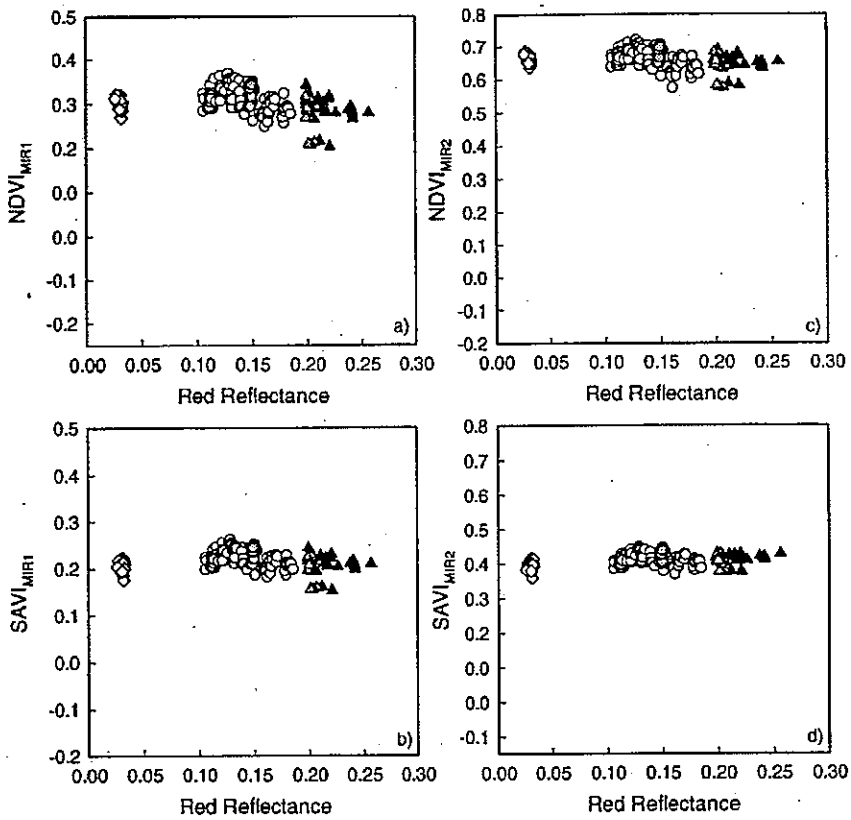


**Figure 4.** Middle-infrared (MIR) derived VIs plotted against red reflectances for forested areas. The legend is the same as in Figure 2. The open circles are for pixels extracted under variable smoke contamination.

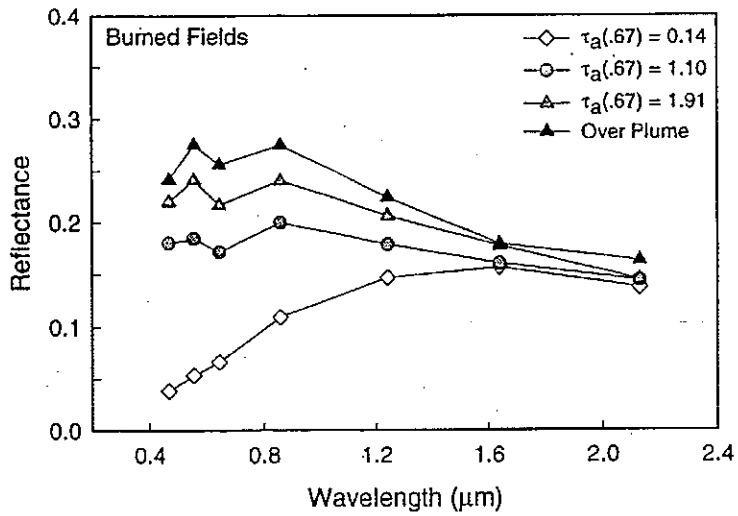


**Figure 5.** Rayleigh/ozone-corrected reflectance spectra of burned fields under four different smoke contaminations. The spectra were extracted near the Sun photometer sites except for the one over the plume.

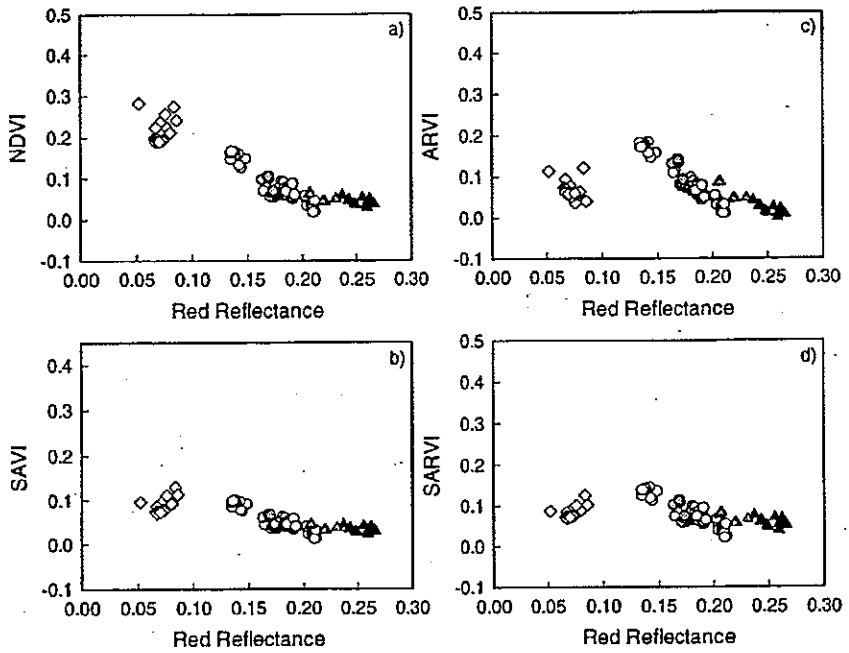


**Figure 6.** NDVI, SAVI, and atmospheric resistant VIs plotted against red reflectances for burned fields. The legend is the same as in Figure 5. The open circles are for pixels extracted under variable smoke contamination.

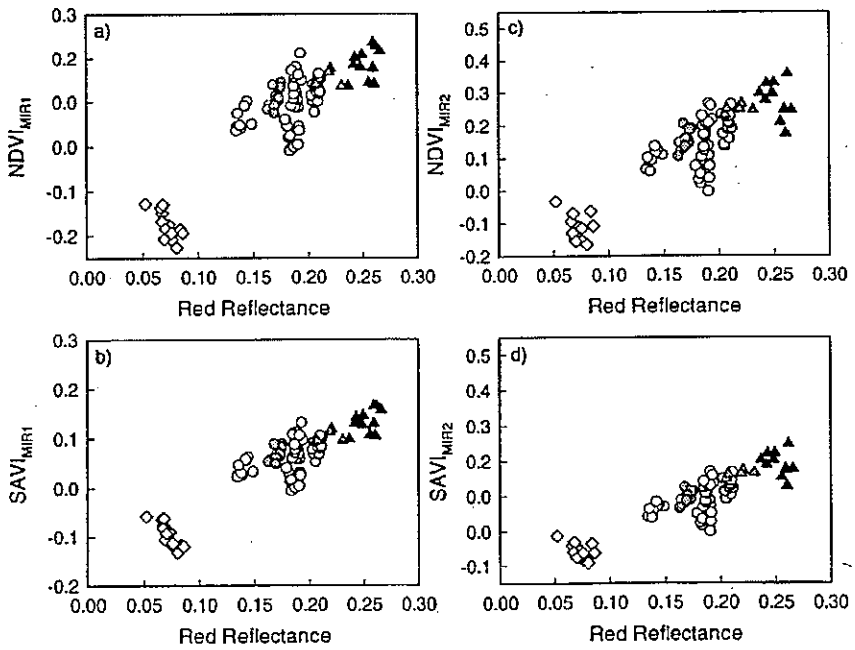


**Figure 7.** MIR-derived VIs plotted against red reflectance for burned fields. The legend is the same as in Figure 5. The open circles are for pixels extracted under variable smoke contamination.

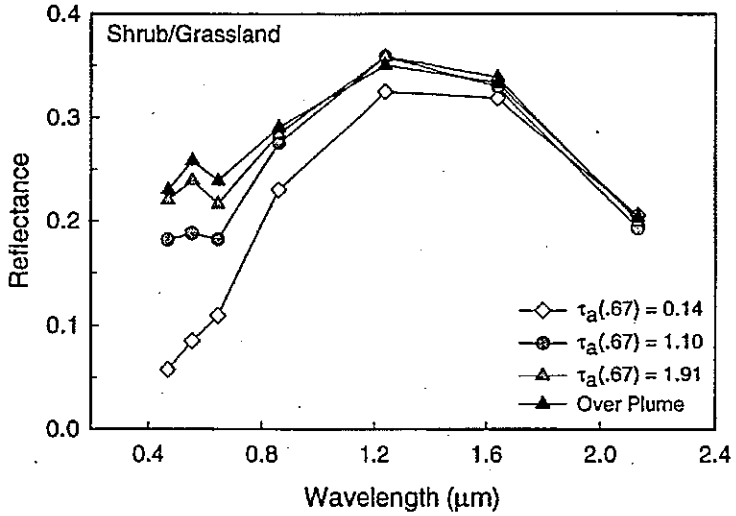


**Figure 8.** Rayleigh/ozone-corrected reflectance spectra for shrub/grasslands under four different smoke contaminations. The spectra were extracted near the Sun photometer sites except for the one over the plume.

5%), outperforming the atmospheric resistant VIs (Figure 10a). The MIR-derived VIs also had nearly constant errors with increasing aerosol optical thickness, while the NDVI, SAVI, and atmospheric resistant VIs had increasing relative errors with higher levels of smoke (Figure 10a). The atmospheric resistant VIs were less affected by smoke than their nonresistant equations, NDVI and SAVI, particularly at AOT at 0.67 μm of 1.10 where the SARVI approached a 10% relative error (Figure 10a). The SARVI performed the best with an average error of 37% among the indices not utilizing a MIR band, while there were essentially no significant differences among the MIR-derived VIs.

The NDVI, SAVI, and their atmospheric resistant variants performed better than the MIR-derived VIs over the burned fields, with the NDVI at 21% average error, the SAVI at 11% average error, and their atmospheric resistant variants below

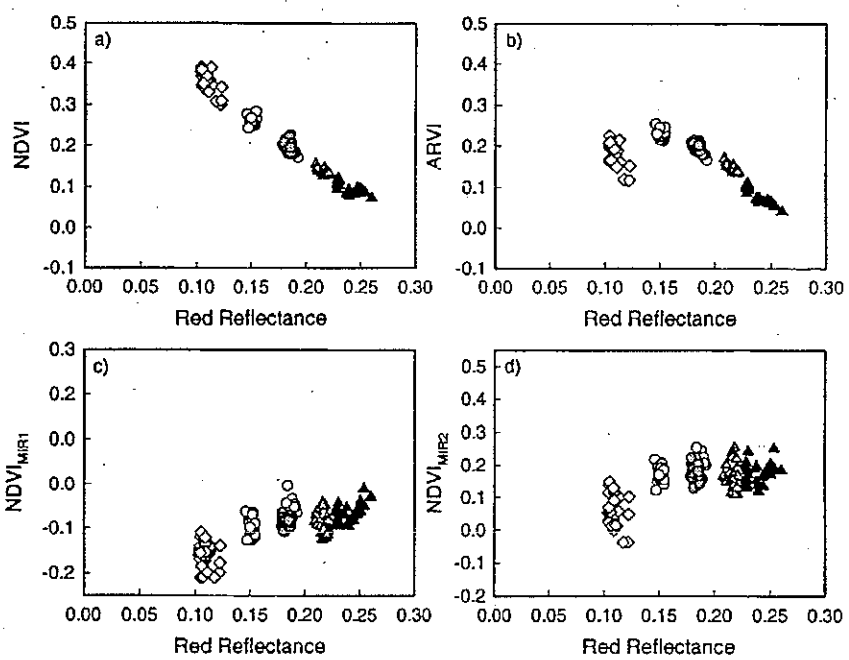


**Figure 9.** NDVI, atmospherically resistant vegetation index (ARVI), and MIR-derived NDVI plotted against red reflectance for shrub/grasslands. The legend is the same as in Figure 8. The open circles are for pixels extracted under variable smoke contamination.

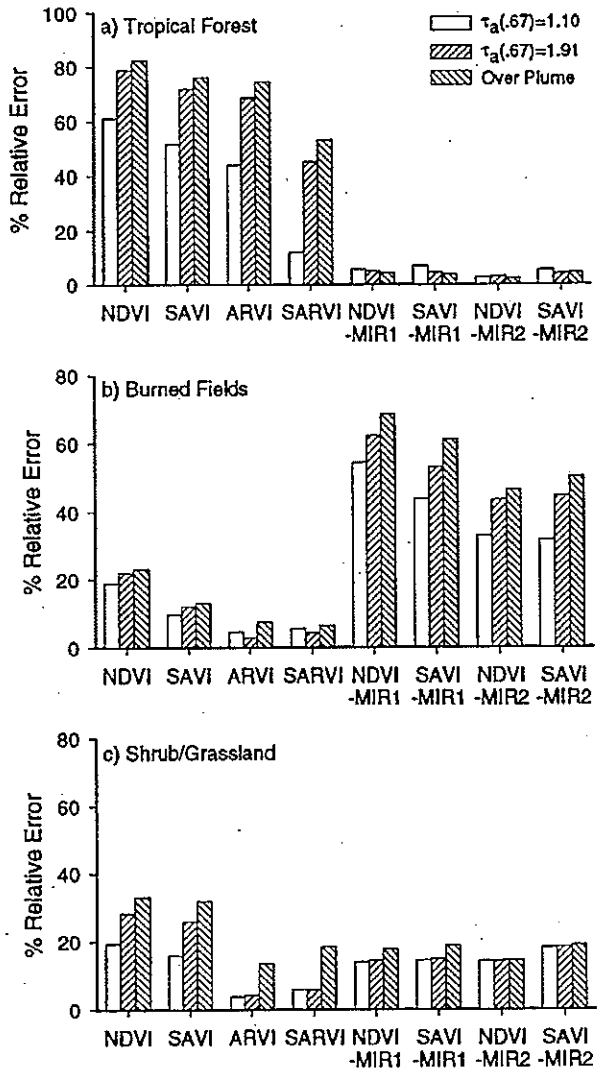


**Figure 10.** Comparisons of percent relative errors among VIs for (a) forested areas, (b) burned fields, and (c) shrub/grasslands.

6% (Figure 10b). The NDVI and SAVI had increasing relative errors with increasing aerosol optical thickness while the atmospheric resistant VIs had the smallest error at AOT at 0.67 μm of 1.91 (Figure 10b). Among the MIR-derived VIs, the MIR2-derived VIs showed smaller relative errors (~ 40%) than the MIR1-derived VIs (> 50%) (Figure 10b). All of the MIR-derived indices had increasing relative errors with increasing aerosol optical thickness (Figure 10b).

For the shrub/grassland site, the atmospheric resistant VIs showed smaller errors (7 and 10% average errors for ARVI and SARVI, respectively) than the MIR-derived VIs (≥ 14% average errors) (Figure 10c). However, the MIR-derived VIs had relative errors invariant to the aerosol optical thickness, while the atmospheric resistant VIs had larger errors at the maximum aerosol optical thickness (over the smoke plume) (Figure 10c). There were no significant differences among the MIR-derived VIs except for the slightly larger errors in the MIR1-derived VIs over the smoke plume (Figure 10c). The NDVI and SAVI had the worst relative errors (> 25%), and all of the VIs exhibited relative errors intermediate in values between the densely vegetated tropical forest and the nearly barren, burned fields (Figure 10).

In Figures 11 and 12, all land cover types are plotted for each index to compare VI behavior throughout its dynamic range. The NDVI of each land cover type decreased linearly with increasing red reflectances (higher levels of smoke) (Figure 11a). The NDVI values of smoke-contaminated vegetated pixels (forest and shrub/grassland) were mostly below the NDVI values of the burned fields under clear sky conditions (minimal vegetation), indicating that one would not be able to sense vegetation in smoke-filled areas with the NDVI. This situation also occurred, but to a much lesser extent, with the SAVI (Figure 11b) and did not occur with the atmospheric resistant VIs (Figures 11c, 11d). Thus the NDVI values of the forested areas over intermediate levels of smoke (red reflectance ~ 0.17) became as low as over the burned fields under clear sky conditions (Figure 11a). This was also the case for the SAVI but at higher levels of smoke contamination (red reflectance ~ 0.22) (Figure 11b). The ARVI values dropped to these of the burned fields only over the smoke plume, while the SARVI values of the forest did not become as low as the burned fields throughout the range of aerosol optical thickness examined here (Figures 11c, 11d).

One can observe the relative constant values of the MIR-derived VIs over the forest sites due to the invariancy to smoke levels (Figure 12). However, the burned fields and shrub/grass areas increased in VI values with increasing levels of smoke (Figure 12). There were significant differences between the MIR1 and MIR2-derived VIs. The MIR1-derived VIs had higher values over the burned fields than over the shrub/grasslands, with the former values reaching the values over the forested areas at the maximum aerosol optical thickness (Figure 12). The MIR2-derived VIs had better separation of the forested areas from the other two land cover types but were unable to distinguish burned fields from shrub/grassland (Figure 12).

## 4. Conclusions and Discussion

We evaluated the performance of the atmospheric resistant and MIR-derived VIs in smoke-filled atmospheres for vegetation detection and monitoring during the burning season in the Amazon region. The performance of the NDVI and SAVI were also evaluated for comparison. The VIs were analyzed over open tropical forest, burned fields, and shrub/grassland land cover types.

The visible bands were the most seriously affected by smoke, with the blue band containing little surface information over optically thick levels of smoke (AOT at 0.67 μm ≥ 1.10). The NIR reflectances were less affected, although the smoke-contaminated atmospheres reduced the contrasts among the forest and nonforest targets in the NIR reflectances. Thus darker areas increased in NIR reflectances, while brighter targets did not change at all. The MIR bands, on the other hand, penetrated all levels of smoke contamination, revealing nearly all land cover surfaces.

The atmospheric resistant VIs performed well over optically thin smoke (AOT at 0.67 μm < 1.10) but not over optically thick smoke (AOT at 0.67 μm ≥ 1.10). Their values

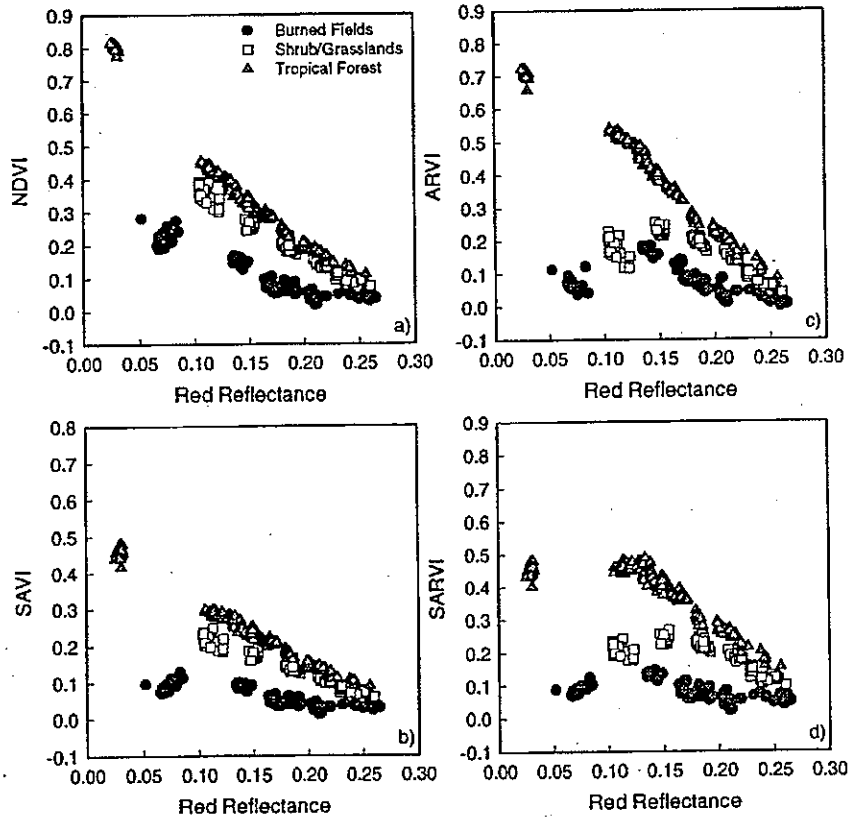


**Figure 11.** NDVI, SAVI, and atmospheric resistant VIs plotted against red reflectances.

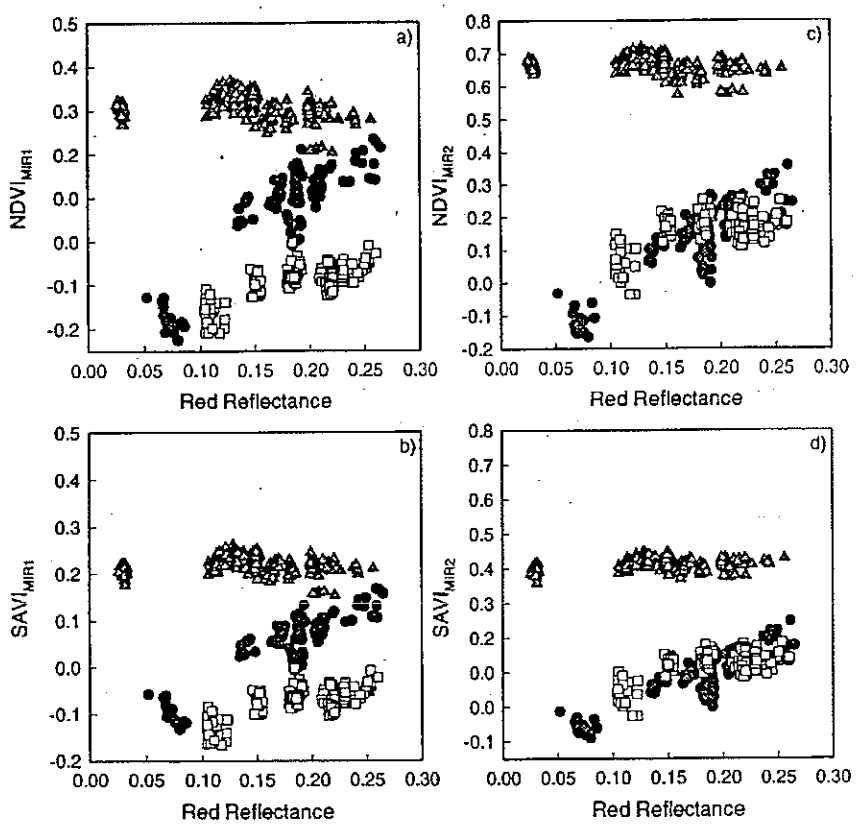


**Figure 12.** MIR-derived VIs plotted against red reflectances. The legend is the same as in Figure 11.

decreased with increasing smoke contamination. The MIR-derived VIs outperformed all the NDVI, SAVI, and atmospheric resistant VIs over the forested areas but were somewhat limited in lower biomass conditions. Over these areas, smoke raised the NIR reflectances and caused an increase in the MIR-derived VI values with increasing aerosol optical thickness. The MIR indices were also found to be highly sensitive to surface variations. The scatter encountered with the MIR indices were higher than with the NDVI and SAVI due to the higher penetration capability of the MIR bands, thus capturing more of the surface variations. These variations may have been associated with moisture, structure, roughness, and canopy background variations over the three sites. Among the MIR indices, the MIR2-derived VIs resulted in better separation of the forested areas from the other two land cover types than the MIR1-derived VIs but were unable to distinguish the burned fields from the shrub/grassland. Thus the MIR-derived VIs, particularly with MODIS band 7 (2.13 μm), are useful in vegetation monitoring over forests during the burning season, but they can only be applied to densely vegetated areas.

Despite its usefulness over forested areas, the results of this study raise concerns for the effective, operational use of MIR bands for vegetation monitoring. One concern is that the NIR band remains sensitive to smoke and causes higher MIR-derived VI values over burned fields and shrub/grassland with smoke contamination. Use of the second, NIR2 band (MODIS band 5, 1.24 μm), in place of the NIR band, may be considered, however, this band is also affected by thick smoke as seen in Figure 5. In addition, NIR2 reflectances of green vegetation do not necessarily correlate with NIR reflectances [*Elvidge*, 1990]. Unless the smoke aerosol effects on the NIR band can be corrected, the MIR bands with the current VI equations (equations 6 and 7) may not be applicable to a wide range of land cover conditions. The MODIS fire products would alert us to potential problems such as burned areas. Another concern is the secondary variations (scatter) encountered with the MIR-derived VIs at all sites, which remain unclear in this study. We suspect that these are associated with "real" surface variations, observed with the smoke-transparent, MIR bands. In this case, a combination of more than two bands, such as MODIS bands 5, 6, and 7, may yield additional information useful in vegetation monitoring.

## References


Andreae, M. O., Biomass burning: Its history, use, and distribution and its impact on environmental quality and global climate, in *Global Biomass Burning-Atmospheric, Climatic, and Biospheric Implications*, edited by J.S. Levine, MIT Press, Cambridge, Mass., 1991.

Crutzen, P. J., and M. O. Andreae, Biomass burning in the tropics: Impact on atmospheric chemistry and biogeochemical cycles, *Science*, *250*, 1669-1678, 1990.

Goward, S. N., B. Markham, D. G. Dye, W. Dulaney, and J. Yang, Normalized difference vegetation index measurements from the Advanced Very High Resolution Radiometer, *Remote Sens. Environ.*, *35*, 257-277, 1991.

Elvidge, C. D., Visible and near infrared reflectance characteristics of dry plant materials, *Int. J. Remote Sens.*, *11*, 1775-1795, 1990.

Hao, W. M., M. H. Liu, and P. J. Crutzen, Estimates of annual and regional releases of $CO_2$ and other trace gases to the atmosphere from fires in the tropics, based on the FAO statistics for the period 1975-1980, in *Fire in the Tropical Biota*, edited by J.G. Goldammer, Springer-Verlag, New York, 1990.

Holben, B. N., T. F. Eck, A. Setzer, I. Slutsker, A. Pereira, B. Markham, and J. V. Castle, Temporal and spatial variability of aerosol loading and properties during the Amazon, North American temperate, and boreal forest burning seasons, in *Biomass Burning and Global Change, vol. II*, edited by J.S. Levine, MIT Press, Cambridge, Mass., 1996.

Huete, A. R., A soil-adjusted vegetation index (SAVI), *Remote Sens. Environ.*, *25*, 295-309, 1988.

Huete, A. R., C.O. Justice, and H.Q. Liu, Development of vegetation and soil indices for MODIS-EOS, *Remote Sens. Environ.*, *49*, 224-234, 1994.

Huete, A. R., H. Q. Liu, K. Batchily, and W. van Leeuwen, A comparison of vegetation indices over a global set of TM images for EOS-MODIS, *Remote Sens. Environ.*, *59*, 440-451, 1997.

Justice, C. O., J. R. G. Townshend, B. N. Holben, and C. J. Tucker, Analysis of the phenology of global vegetation using meteorological satellite data, *Int. J. Remote Sens.*, *6*, 1271-1318, 1985.

Kaufman, Y. J., and L. A. Remer, Detection of forests using mid-IR reflectance: An application for aerosol studies, *IEEE Trans. Geosci. Remote Sens.*, *32*, 672-683, 1994.

Kaufman, Y. J., and D. Tanré, Atmospherically resistant vegetation index (ARVI) for EOS-MODIS, *IEEE Trans. Geosci. Remote Sens.*, *30*, 261-270, 1992.

Kaufman, Y. J., C. J. Tucker, and I. J. Fung, Remote sensing of biomass burning in the tropics, *J. Geophys. Res.*, *95*, 9927-9939, 1990.

Sellers, P. J., C. J. Tucker, G. J. Collatz, et al., A global 10 * 10 NDVI data set for climate studies, 2, The adjustment of the NDVI and generation of global fields of terrestrial biophysical parameters, *Int. J. Remote Sens.*, *15*, 3519-3545, 1994.

Tanré, D., B. N. Holben, and Y. J. Kaufman, Atmospheric correction algorithm for NOAA-AVHRR products: Theory and application, *IEEE Trans. Geosci. Remote Sens.*, *30*, 231-248, 1992.

Townshend, J. R. G., C. Justice, W. Li., C. Gurney, and J. McManus, Global land cover classification by remote sensing: present capabilities and future possibilities, *Remote Sens. Environ.*, *35*, 243-256, 1991.

Tucker, C. J., Red and photographic infrared linear combinations for monitoring vegetation, *Remote Sens. Environ.*, *8*, 127-150, 1979.

Vermote, E., D. Tanré, J. L. Deuze, M. Herman, and J. J. Morcrette, Second simulation of the satellite signal in the solar spectrum (6S), in *6S User Guide Version 1*, 216 pp., LOA-USTL, Villeneuve d'Ascq, France, 1995.


K. Didan, A. R. Huete, W. J. D. van Leeuwen, and T. Miura (corresponding author), Department of Soil, Water and Environmental Science, University of Arizona, 429 Shantz Bldg., #38, Tucson, AZ 85721. (e-mail: tomoaki@ag.arizona.edu)

(Received September 10, 1997; revised December 16, 1997; accepted December 18, 1997)